industries

MDPI

Article

Mode Prioritization for Vibration-Based Condition Monitoring: A Laboratory Sensitivity and Consistency Assessment of Damaged Aluminum Cantilever Beams

Georgios Samourgkanidis

Department of Civil and Environmental Engineering, University of Cyprus, Nicosia 1678, Cyprus; samourgkanidis.georgios@ucy.ac.cy

Abstract

Vibration-based condition monitoring of beam-like metallic components requires vibration modes that are both sensitive to damage and consistent across different damage locations and severities. This study evaluates the damage sensitivity of the first eight bending-mode frequencies measured from 19 aluminum-alloy 6063 cantilever beams instrumented with magnetoelastic vibration sensors. The examined configurations comprised one undamaged reference beam and 18 damaged beams combining 6 six crack-like defect locations with three defect depths. Normalized absolute frequency shifts were used to determine the mean sensitivity of each mode, its response to increasing defect depth, and the consistency of this response across the examined locations. The combined modal response increased progressively with defect depth, although the magnitude of the change depended on the selected mode and defect location. Mode f_7 exhibited the highest mean sensitivity (1.234%), comparable to f_5 and f_6, and a monotonic-consistency ratio of $C_7 = 1$, indicating an increasing response with defect depth at all six locations. Modes f_2 and f_4 also demonstrated complete monotonic consistency but lower overall sensitivity, whereas f_5 showed comparatively high sensitivity with greater dependence on defect location. Mode f_8 presented the lowest sensitivity and consistency. The results show that high sensitivity does not guarantee consistent depth-dependent behavior (f_5), so both criteria are needed to prioritize modes. Prioritizing modes that combine high sensitivity with consistent depth-dependent behavior may simplify the processing of modal information in laboratory studies of beam-like metallic components. Because the specimens were idealized beams with a single machined defect, validation on independent specimens, realistic damage, and operational and environmental conditions is required before diagnostic thresholds or practical monitoring applications can be considered.

Keywords: condition monitoring; modal analysis; magnetoelastic sensors; modal sensitivity; aluminum beams; structural health monitoring

Check for updates

Academic Editor: Ying Liu

Received: 2 September 2026
Revised: 18 October 2026
Accepted: 30 October 2026
Published: 6 November 2026

Copyright: © 2026 by the author. Licensee MDPI, Basel, Switzerland. This article is an open access article distributed under the terms and conditions of the Creative Commons Attribution (CC BY) license.

1. Introduction

The safe and reliable operation of engineering structures and components is essential to the performance and sustainability of modern industrial systems. Throughout their service life, structural components are exposed to mechanical loading, environmental influences, material degradation, and other factors that may progressively compromise their integrity and functional performance [1]. If such deterioration is not identified at an early stage, it may result in increased maintenance requirements, unexpected downtime, reduced service

life, and, in severe cases, structural failure. For this reason, the effective assessment of structural condition has become an important element of maintenance and asset-management strategies across a wide range of industrial applications [2]. Consequently, the development of monitoring approaches capable of identifying changes in structural condition in a reliable, practical, and timely manner is of considerable importance for supporting safer operation, more efficient maintenance planning, and improved utilization of engineering assets [3]. Within this broader context, structural health monitoring (SHM) has emerged as a systematic framework for assessing structural condition through the acquisition, processing, and interpretation of measured response data over time [4–7]. By complementing conventional inspection and non-destructive 38 evaluation procedures, SHM can enable more frequent or continuous observation of structural behavior and provide information for damage detection, condition assessment, and maintenance-related decision making [8,9]. Advances in sensing technologies, wireless communication, data-acquisition systems, and intelligent monitoring architectures have further expanded the capabilities of SHM, facilitating distributed, remote, and increasingly automated monitoring of engineering structures [10–12]. Nevertheless, the practical effectiveness of an SHM system depends not only on the availability of sensing technologies [13], but also on appropriate sensor selection, measurement quality, deployment conditions, data management, and the ability to extract reliable condition-sensitive information from the acquired signals [14]. Within this broad monitoring framework, vibration-based approaches have become one of the principal means of evaluating structural condition through changes in measured dynamic response.

Among the different strategies employed within SHM, vibration-based approaches have been widely investigated because the dynamic response of a structure is directly related to its underlying physical and mechanical properties [15–17]. Several comprehensive reviews have classified vibration-based condition-assessment methods according to the measured dynamic characteristics and the intended level of damage identification [18–21]. The presence of damage, particularly when associated with a local reduction in stiffness, can modify the vibration characteristics of a structural system and thereby produce changes in measurable dynamic features. Consequently, modal parameters such as natural frequencies, mode shapes, and damping ratios, as well as frequency response functions, have been extensively explored as damage-sensitive quantities for structural condition assessment [22,23]. Their extraction may be performed under controlled excitation or from measured structural responses under operational and ambient conditions, extending the applicability of vibration-based monitoring from laboratory investigations to in-service structures [24,25]. However, the interpretation of modal changes in practical applications remains challenging because the identified dynamic characteristics may also be influenced by environmental and operational variability, measurement noise, and uncertainties associated with modal-parameter estimation [24,26]. The selection of dynamic features that are sufficiently sensitive to structural changes while remaining suitable for reliable interpretation is therefore an important consideration in the development of vibration-based condition-monitoring strategies.

Natural-frequency-based approaches have been investigated extensively for the detection and characterization of localized damage in beam-like structures, where a crack introduces a local reduction in stiffness that can alter the modal frequencies of the system [27–29]. Earlier studies demonstrated that variations in natural frequencies could be used to estimate crack location and severity through optimization-based and model-based procedures [30–35]. Subsequent experimental investigations [36] further demonstrated the applicability of measured modal frequencies for identifying cracks in beams with different geometries, boundary conditions, and damage configurations [37,38]. Magnetoelastic resonance sensors permit remote and contactless interrogation because their mechanical

response can be detected magnetically [39]. In this context, Samourgkanidis and Kouzoudis introduced magnetoelastic ribbons as vibration sensors with contactless magnetic readout for measuring bending-mode frequencies in aluminum cantilever beams, demonstrating experimentally that both crack location and crack depth influence the measured modal response [40]. The approach was subsequently extended to the identification of transverse cracks using the first eight bending modes of aluminum-alloy 6063 cantilever beams and a pattern-matching procedure based on normalized modal frequencies [41]. Further investigations characterized the sensing performance of magnetoelastic ribbons using the natural frequencies of cantilever beams and demonstrated their applicability to vibration monitoring of rotating metallic beam-like components [42,43]. The applicability of contactless magnetoelastic modal sensing was also broadened through the use of embedded ribbons in additively manufactured polymer beams and through damage-monitoring studies on cementitious and concrete beams employing ribbon and microwire sensing elements [44–47]. Collectively, these studies demonstrate the potential of natural-frequency information for damage assessment while also indicating that the magnitude of the modal response is influenced by the particular damage configuration and the vibration mode considered. An important characteristic of frequency-based damage assessment is that the measured modal response depends not only on the severity of damage but also on its location and on the vibration mode considered. For beam-like structures, a defect of a given size may produce markedly different changes in different modes because the influence of a local stiffness reduction depends on the deformation characteristics of each mode at the damaged position [48,49]. Accordingly, cracks located near regions of low modal curvature may have only a limited influence on a particular modal frequency, whereas the same damage can produce a considerably stronger response in another mode or at another structural location [49,50]. Increasing crack depth generally produces a greater reduction in local stiffness and consequently larger changes in natural frequencies, although the magnitude of this effect remains dependent on crack position and modal order [51–53]. Experimental investigations have further shown that the sensitivity of individual modal quantities can vary substantially across damage configurations, motivating the use of information from several modes for damage localization and severity assessment [54,55]. More recent modal-testing studies have similarly reported different levels of responsiveness between lower and higher modes as crack location and depth are varied [56]. These observations indicate that the available vibration modes cannot necessarily be regarded as equally informative for damage assessment, and that their individual sensitivity to changes in damage condition should be considered when selecting modal information for condition-monitoring applications.

Previous studies have demonstrated that the usefulness of modal information for damage assessment is not necessarily uniform across all available modes, leading to the development of approaches based on modal sensitivity, feature selection, or combinations of selected dynamic characteristics [57–61]. Selecting informative modal features may reduce redundant information and simplify subsequent damage assessment while retaining the characteristics most responsive to structural changes [60,62–64]. However, mode-selection strategies have commonly emphasized response magnitude, optimization performance, or diagnostic capability, while comparatively less attention has been directed toward jointly considering whether a mode exhibits both a sufficiently strong damage response and a consistent progression of that response with increasing damage severity across different damage locations [58–61]. The present study addresses this by evaluating each of the first eight bending modes individually using two complementary criteria: mean absolute relative frequency shift and a monotonic-consistency ratio across six defect locations. The measurements are those reported in [41], where they were analyzed jointly through pattern matching; here they are re-analyzed to support a preliminary, laboratory-scale prioritization

of modes in aluminum cantilever beams containing a single crack-like defect. The dataset is not new; the contribution of this work is the joint sensitivity-consistency screening of individual modes, which complements the joint pattern-matching analysis of [41] by indicating which modes carry the most reliable depth-dependent information. The results are a preliminary laboratory-scale screening, not a validated monitoring method.

2. Materials and Methods

The investigated dataset consisted of 19 aluminum-alloy 6063 cantilever beams: one undamaged reference beam and 18 beams containing a single crack-like defect. Each beam had a total length of 400 mm, including a free length of 350 mm and a clamped length of 50 mm. The cross-section had a width of 30.25 mm and a thickness of 8.18 mm. The nominal density and elastic modulus of the material were 2.69 g/cm^3 and 68.3 GPa, respectively. All specimens were manufactured to the same nominal dimensions using CNC machining. The damaged beams represented combinations of six defect locations and three defect depths.

The defects were positioned at distances of 50, 100, 150, 200, 250, and 300 mm from the clamped end. At each location, depths of 1, 2, and 3 mm were examined, resulting in 18 damage configurations. The defects had a nominal width of 1 mm and a V-shaped termination and were used as controlled representations of localized damage in beam-like metallic components (Figure 1). The bending-mode frequencies were measured using two Metglas 2826MB3 magnetoelastic ribbons as vibration sensors (Conway, SC, USA). Each ribbon was 100 mm long, 6 mm wide, and approximately 29 µm thick, and both were attached near the free end of the beam. During the measurements, one end of each beam was clamped between appropriately shaped plates using a CARVER hydraulic press (Carver, Inc., Wabash, IN, USA). The beam was excited by a mechanical stimulator driven by a Keithley 3390 50 MHz arbitrary waveform generator (Keithley Instruments, Cleveland, OH, USA) through a MAC 2.2 stereo power amplifier (Alto Professional, Cumberland, RI, USA) and was then left to vibrate freely (The experimental setup is described in detail in [41]). The resulting deformation of the magnetoelastic ribbons produced variations in their magnetization, which induced a voltage in a nearby pickup coil. The pickup-coil signal was transferred to a computer through the microphone input of a sound card. Each signal was recorded for 10 s at a sampling frequency of 48 kHz. The corresponding frequency spectra were obtained using the fast Fourier transform in MATLAB R2021b (MathWorks, Natick, MA, USA) software, providing a frequency resolution of 0.1 Hz. The first eight identifiable bending-mode frequencies, denoted by f_1–f_8, were extracted within the frequency range from 0 to 9 kHz. The modal-frequency measurements analyzed in the present study were obtained during the experimental work described in [41] and are summarized in Table 1. The specimens were idealized laboratory beams, each containing a single machined crack-like defect, measured in a laboratory setting with one end fixed. The study therefore does not address operational loads, temperature variations, changes in connection conditions, external vibration sources, or other environmental variables. The undamaged beam was used as the reference condition. The normalized frequency shift in mode i for damage configuration j was calculated as

$$\Delta f_{i,j}(\%) = \frac{f_{i,0} - f_{i,j}}{f_{i,0}} \times 100 \quad (1)$$

where $f_{i,0}$ is the frequency of mode i for the undamaged beam and $f_{i,j}$ is the corresponding frequency for damaged configuration j. Positive values represent frequency reductions relative to the undamaged condition, whereas negative values represent frequency increases.

To assess the magnitude of the modal response independently of its direction, the absolute relative frequency shift was used as the sensitivity indicator:

$$S_{i,j} = |\Delta f_{i,j}| \tag{2}$$

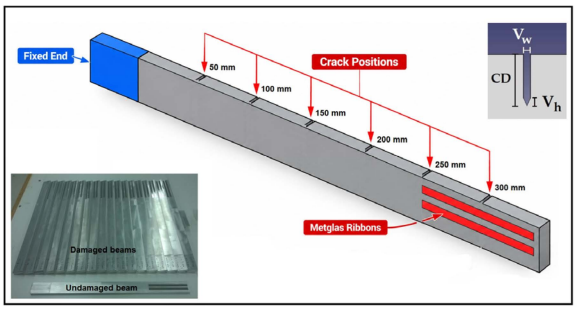


Figure 1. Schematic of the cantilever beam showing the fixed end, six defect positions, and Metglas ribbons. The inset illustrates the defect geometry ((V_w) = 1 mm, (V_h) = 0.5 mm, and CD = 1, 2, and 3 mm), while the bottom-left image shows the actual beam specimens (Adapted from [41]).

Table 1. Beam configurations and measured bending-mode frequencies. U00 denotes the undamaged reference specimen; x denotes the defect distance from the clamped end, and a denotes the defect depth. Each frequency is the mean of five repeated measurements of the same clamped beam.

Specimen	x (mm)	a (mm)	Bending Modes (Hz)							
			$f1$	$f2$	$f3$	$f4$	$f5$	$f6$	$f7$	$f8$
U00	–	–	54.1	337.7	943.2	1840.9	3026.2	4493.5	6226.0	8205.3
D050-1	50	1	53.8	337.7	943.8	1837.3	3014.3	4471.7	6205.7	8199.5
D050-2		2	52.7	336.7	944.1	1829.3	2981.5	4433.9	6173.8	8186.8
D050-3		3	50.9	335.1	944.0	1810.4	2919.7	4371.7	6120.8	8168.2
D100-1	100	1	53.9	337.8	940.1	1838.1	3025.7	4474.7	6202.7	8207.4
D100-2		2	53.4	337.2	930.9	1831.1	3026.0	4436.1	6151.6	8203.3
D100-3		3	52.5	336.4	916.6	1817.4	3025.0	4384.0	6100.3	8197.8
D150-1	150	1	53.9	336.2	943.7	1839.3	3028.2	4494.6	6216.0	8207.6
D150-2		2	53.7	333.0	940.7	1825.9	2999.1	4487.7	6186.1	8206.0
D150-3		3	53.2	326.6	936.6	1805.7	2959.9	4475.5	6038.4	8202.8
D200-1	200	1	54.0	335.6	941.5	1837.7	3018.4	4492.5	6208.3	8207.1
D200-2		2	53.9	331.8	938.9	1827.3	2992.5	4492.9	6162.2	8204.0
D200-3		3	53.7	324.1	931.6	1811.1	2948.6	4483.9	6019.0	8198.0
D250-1	250	1	54.0	336.2	935.8	1835.0	3030.2	4478.0	6204.1	8224.8
D250-2		2	54.0	334.4	923.9	1823.5	3027.6	4442.5	6175.7	8213.2
D250-3		3	54.0	330.3	901.1	1806.7	3029.5	4386.1	6042.1	8191.3
D300-1	300	1	54.0	337.8	942.8	1836.8	3015.9	4472.7	6221.9	8230.6
D300-2		2	54.1	337.5	938.9	1818.3	2974.0	4420.7	6181.9	8182.5
D300-3		3	54.1	336.6	930.5	1785.0	2848.2	4329.2	6074.8	8161.6

For each bending mode, the mean absolute frequency shift was calculated across the 18 damage configurations. The overall sensitivity of mode i was expressed as

$$\overline{S}_i = \frac{1}{18}\sum_{j=1}^{18} S_{i,j} \tag{3}$$

The modes were ranked according to their mean absolute frequency shifts, with higher values indicating a stronger overall response to the examined damage configurations. The influence of damage severity was subsequently examined by grouping the configurations according to defect depth. For this analysis, $S_{i,\ell,d}$ denotes the absolute frequency shift in mode i at defect location ℓ and defect depth d. The mean response of mode i at depth d, averaged across the six defect locations, was calculated as:

$$\overline{S}_{i,d} = \frac{1}{6}\sum_{l=1}^{6} S_{i,l,d} \quad d \in \{1,2,3\}\ \text{mm} \tag{4}$$

To evaluate the overall relationship between defect depth and modal response, the combined sensitivity at each depth was calculated by averaging the absolute shifts across all eight modes and six locations:

$$\overline{S}_{d} = \frac{1}{48}\sum_{i=1}^{8}\sum_{l=1}^{6} S_{i,l,d} \tag{5}$$

The consistency of the depth-dependent response was evaluated separately for every mode and defect location. The response of mode i at location ℓ was classified as monotonic when:

$$S_{i,l,1\ \text{mm}} \le S_{i,l,2\ \text{mm}} \le S_{i,l,3\ \text{mm}} \tag{6}$$

For each mode, the monotonic-consistency ratio was calculated as

$$C_i = \frac{n_i}{6} \tag{7}$$

where n_i is the number of defect locations satisfying the monotonic condition and six is the total number of examined locations. A value of $C_i = 1$ therefore indicates that the absolute frequency shift increased monotonically with defect depth at all six locations. Mean sensitivity and monotonic consistency were interpreted jointly, rather than combined into a weighted index, to distinguish modes showing strong overall responses from modes that followed increasing damage severity more consistently.

All calculations were performed using formula-based spreadsheet analysis. The frequency values listed in Table 1 were analyzed without exclusion, imputation, or additional numerical modification.

Each beam was measured five times in a single clamping, without re-clamping between measurements, and the frequencies listed in Table 1 are the mean values of these five measurements. The repeatability error of the measurements was below 1 Hz. Relative to the frequency of each mode, this corresponds to approximately 1.8% for f_1, 0.3% for f_2, 0.1% for f_3, and below 0.06% for f_4–f_8, so that the relative uncertainty is largest for the lowest modes, whose frequency shifts are the smallest. This error does not include variability associated with re-clamping, sensor attachment, or differences between specimens, since each damage configuration was represented by a single specimen that was clamped once and compared with a single undamaged reference beam, without paired pre-damage baselines. The analysis was therefore descriptive and focused on relative frequency changes, sensitivity ranking, depth-dependent behavior, and response consistency. Consequently, no inferential statistical tests, confidence intervals, diagnostic thresholds, or claims concerning damage-classification accuracy were applied. To examine the influence of the repeatability error on the consistency ratio, C_i was also recalculated with two additional criteria: a lenient criterion, in which a decrease in less than 1 Hz in the absolute frequency shift between successive depths was not counted as a violation of Equation (6), and a strict criterion, in which the absolute frequency shift was required to increase by at least 1 Hz from 1 to 2 mm and from 2 to 3 mm.

3. Results and Discussion

The mean absolute relative frequency shifts differed among the eight bending modes, as shown in Figure 2. The mean modal sensitivity ranged from 0.150% to 1.234%. Mode f_7 exhibited the highest mean absolute shift of 1.234%, followed by f_5 and f_6, with corresponding values of 1.154% and 1.059%, respectively. Mode f_1 ranked fourth with a mean shift of 1.027%. Modes f_4, f_2, and f_3 presented similar intermediate responses of 0.967%, 0.954%, and 0.929%, respectively. In contrast, f_8 exhibited a markedly lower mean sensitivity of 0.150%, clearly separating it from the other modes. Indeed, the sensitivities of modes f_1 through f_7 were confined to a relatively narrow interval between 0.929% and 1.234%, whereas the response of f_8 was substantially lower. Based on the mean absolute frequency shift, the resulting sensitivity order was $f_7 > f_5 > f_6 > f_1 > f_4 > f_2 > f_3 > f_8$: Given the relative measurement uncertainty reported in Section 2, the positions of the lowest modes in this ranking, particularly f_1, are the least certain. This ranking indicates that the contribution of the individual bending modes to the overall damage response was not uniform. Since each value represents an average across all 18 damage configurations, the ranking should be interpreted as a measure of overall modal sensitivity, averaged over the examined defect locations and depths, rather than sensitivity to a particular defect location or depth, and it depends on the position of the defects relative to the modal curvature of each mode. In 18 of the 144 mode–configuration values of Table 1 (12.5%), the damaged beam showed a higher frequency than the undamaged beam, corresponding to negative Δf in Equation (1); three further values were unchanged. These increases occurred for f_8 (7 values), f_3 and f_5 (4 each), f_2 (2) and f_6 (1), and never for f_1, f_4 and f_7. They were below 1 Hz for f_2 and f_3, between 1.1 and 4.0 Hz for f_5 and f_6, and up to 25.3 Hz for f_8, mostly at 1 mm, where the defect-induced shifts are small. A small mass reduction at low-curvature positions can slightly raise the frequency, but the larger increases, found mainly for f_8, are more likely related to specimen-to-specimen variability, clamping, and sensor installation, which were not quantified.

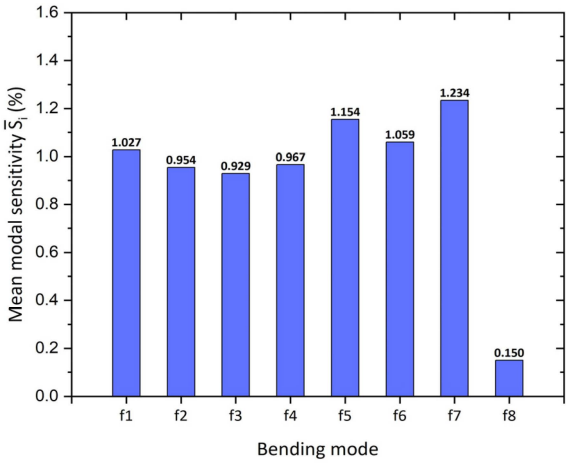


Figure 2. Mean absolute relative frequency shift in each bending mode across the 18 damage configurations.

To check their influence, the sensitivity was recalculated by counting increases as zero and by averaging the signed shifts. The ranking $f_7 > f_5 > f_6 > f_1 > f_4 > f_2 > f_3 > f_8$ was identical in both cases, and the difference between f_7 and f_5 increased from 0.08 to 0.10–0.12 percentage points. The consistency ratios of f_1–f_7 were also unchanged, whereas C_8 would increase to 1 for signed shifts, because the increases in f_8 at 1 mm turn into reductions at 3 mm. The low priority of f_8 therefore rests on its low sensitivity.

Figure 3 presents the mean absolute relative frequency shift in each bending mode at the three defect depths, averaged across the six defect locations. For modes f_1–f_7, the

mean response increased progressively as the defect depth increased from 1 to 3 mm. When averaged across all modes and locations, the combined modal sensitivity increased from 0.234% at 1 mm to 0.749% at 2 mm and 1.820% at 3 mm. Thus, within the examined configurations, deeper defects generally produced larger deviations from the modal frequencies of the undamaged beam. This trend is consistent with the greater disturbance of the local bending stiffness caused by an increase in defect depth. The depth-resolved results also show that the most responsive mode varied with defect depth. Mode f_1 presented the numerically highest mean sensitivity at 1 mm, with a value of 0.308%, whereas f_6 produced the highest response at 2 mm, reaching 0.917%. At 3 mm, f_7 exhibited the largest mean shift of 2.571%, followed by f_5 at 2.384%. Therefore, although f_7 had the highest overall sensitivity in Figure 2, it was not the most responsive mode at every defect depth. Its overall ranking was influenced particularly by its pronounced response to the deepest defects. Mode f_8 behaved differently from the remaining modes, presenting mean shifts in only 0.115%, 0.108%, and 0.228% at depths of 1, 2, and 3 mm, respectively. Its response remained comparatively small across all three depths, supporting the low overall sensitivity observed in Figure 2. These findings demonstrate that modal sensitivity depends on defect depth and that an overall sensitivity ranking alone does not fully describe the behavior of each mode. Nevertheless, because the values in Figure 3 were averaged across the six defect locations, location-specific monotonicity cannot be established from this figure and is examined separately using the monotonic-consistency ratio.

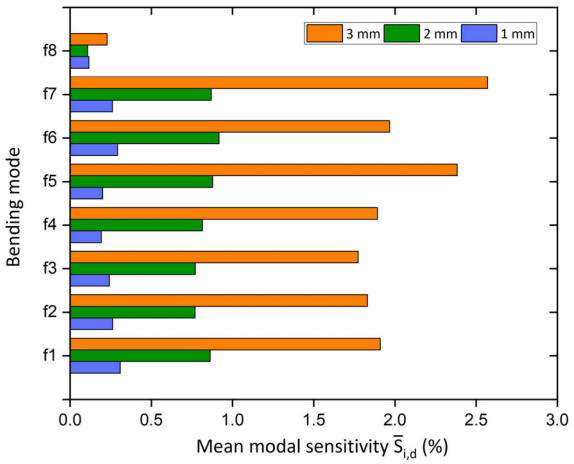


Figure 3. Mean absolute relative frequency shift in each bending mode at defect depths of 1, 2, and 3 mm, averaged across the six defect locations.

The joint representation of mean modal sensitivity and monotonic consistency in Figure 4 provides a more complete comparison of the eight bending modes. Mode f_7 occupied the upper-right region of the graph, combining the highest mean sensitivity of 1.234% with a monotonic-consistency ratio of $C_7 = 1$. This indicates that f_7 combined the highest mean response, which was comparable to those of f_5 and f_6, with increasing absolute frequency shifts with defect depth at all six examined locations. Within the present dataset, f_7 can therefore be regarded as the most balanced candidate for prioritization in a vibration-based monitoring strategy. Modes f_2 and f_4 also achieved complete monotonic consistency, with $C_2 = C_4 = 1$, although their mean sensitivities were lower, at 0.954% and 0.967%, respectively. These modes were less responsive overall than f_7 but followed increasing defect depth consistently and may therefore provide complementary information when monitoring damage progression. In contrast, f_5 exhibited a relatively high mean sensitivity of 1.154% but a lower consistency ratio of $C_5 = 0.667$, corresponding to monotonic behavior at

four of the six locations. Its position in Figure 4 demonstrates that a high average frequency shift does not necessarily imply a consistent response across different defect locations.

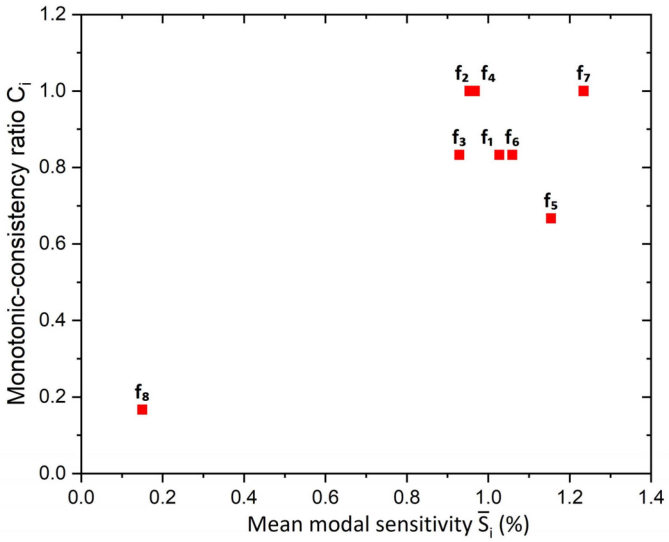


Figure 4. Joint representation of the mean modal sensitivity and monotonic-consistency ratio for the eight bending modes. A value of $C_i = 1$ indicates a monotonic increase in the absolute frequency shift with defect depth at all six examined locations.

Modes f_1, f_3, and f_6 occupied an intermediate region of the graph. Each mode presented a consistency ratio of $C_1 = C_3 = C_6 = 0.833$, corresponding to monotonic responses at five of the six defect locations, while maintaining moderate-to-high mean sensitivities. Mode f_8 was clearly separated from the remaining modes, combining the lowest mean sensitivity of 0.150% with the lowest consistency ratio of $C_8 = 0.167$, which results mainly from its frequency increases at 1 and 2 mm. This indicates that f_8 provided limited information regarding the examined defect configurations and their depth-dependent progression. Table 2 shows the consistency ratios obtained with a lenient and a strict criterion that account for the measurement error of about 1 Hz. In the lenient criterion, a decrease in less than 1 Hz in the absolute frequency shift between successive depths was not counted as a violation of Equation (6), since differences in this size are within the measurement error. Under this criterion, modes f_1, f_2, f_3, f_4, f_6 and f_7 were monotonic at all six locations ($C_i = 1$). For f_1, f_3 and f_6, the single non-monotonic location identified by Equation (6) therefore corresponds to a deviation within the measurement error, and their ratio of 0.833 cannot be distinguished from complete consistency. Mode f_5 increased to $C_5 = 0.833$, because its deviation at 100 mm (0.3 Hz) was within the error, whereas its deviation at 250 mm (shifts of 4.0, 1.4 and 3.3 Hz) exceeded it. Mode f_8 increased to $C_8 = 0.500$ but remained the lowest, since its deviations at 150, 250 and 300 mm were larger than 1 Hz. In the strict criterion, a location was classified as monotonic only if the absolute frequency shift increased by at least 1 Hz from 1 to 2 mm and from 2 to 3 mm, so that every increase was larger than the measurement error. Modes f_4 and f_7 retained $C_i = 1$, indicating that their depth-dependent increase was clearly resolved at all six locations. Modes f_3 and f_6 ($C_i = 0.833$), f_5 ($C_5 = 0.667$) and f_8 ($C_8 = 0.167$) were unchanged from Equation (6). Mode f_2 decreased to 0.667, because its shifts at 100 and 300 mm were small (0.1–1.3 Hz) and its increases between successive depths were below 1 Hz. Mode f_1 decreased to 0.167, since its frequency shifts (0.0–3.2 Hz) were comparable to the measurement error, and its depth dependence could not be reliably resolved. These results indicate that the prioritization of f_7 and the low ranking of f_8 are not caused by the repeatability error of the measurements, although variability due to

clamping, sensor attachment, and differences between specimens was not quantified and may be larger.

Table 2. Monotonic-consistency ratio C_i of each bending mode, calculated with Equation (6), with a lenient criterion (decreases below 1 Hz tolerated) and with a strict criterion (increases of at least 1 Hz required between successive depths).

Mode	C_i	1 Hz Tolerance	Steps ≥ 1 Hz
f1	0.833	1.000	0.167
f2	1.000	1.000	0.667
f3	0.833	1.000	0.833
f4	1.000	1.000	1.000
f5	0.667	0.833	0.667
f6	0.833	1.000	0.833
f7	1.000	1.000	1.000
f8	0.167	0.500	0.167

The mean sensitivities of f_7 (1.234%), f_5 (1.154%) and f_6 (1.059%) are close, and the difference between f_7 and f_5 is only 0.08 percentage points. Two checks were performed to evaluate whether this difference is meaningful. First, to test whether it could be caused by the measurement error alone, independent normally distributed random errors with a standard deviation of 1 Hz were added to every mean frequency in Table 1, including that of the undamaged beam, and the mean sensitivities were recalculated. This was repeated for 20,000 realizations. The difference between the mean sensitivities of f_7 and f_5 remained positive in the 95% interval of 0.03–0.12 percentage points, indicating that it exceeds the repeatability error of the measurements. Second, the dependence of the ranking on the defect configurations was examined.

Mode f_7 exceeded f_5 in only 10 of the 18 configurations: it was larger at 100 and 250 mm and smaller at 50 and 300 mm at all three depths, with mixed results at 150 and 200 mm. Excluding either the 100 mm or the 250 mm location reversed the order of the two modes, and excluding the 3 mm defects made f_6 the most sensitive mode. Excluding any single location left f_7 in first or second place and f_8 in last place, and at individual locations f_7 ranked between second and fourth. Its position therefore results from a response that varies little between locations (location-mean sensitivity of 0.95–1.55%, compared with 0.02–2.65% for f_5) and not from being the most sensitive mode at any location. The mean sensitivities of f_5, f_6 and f_7 should therefore be regarded as comparable, and the present data do not establish the superiority of f_7 in terms of sensitivity alone. The preference for f_7 rests on the combination of this high sensitivity with $C_7 = 1$ under Equation (6) and under both the lenient and strict criteria. Modes f_5 and f_6 did not combine high sensitivity with this consistency ($C_5 = 0.667$–0.833 and $C_6 = 0.833$–1.000), and f_2 and f_4 had lower mean sensitivities. Unlike mode-selection approaches that rely on optimization or identification performance [57–61] and the reduced-parameter method of [65], the proposed screening uses only measured frequencies and two interpretable criteria, and it resolves the response by defect location, so it can be applied as a low-cost pre-screening step before more elaborate methods. A quantitative comparison with those approaches would require mode shapes or numerical models and independent data, and is left for future work.

The mode- and location-dependent response can be interpreted in terms of modal curvature. An defect reduces the local bending stiffness, and the resulting decrease in the natural frequency of a given mode depends on the bending strain energy stored at the defect position, which is governed by the local curvature of the mode shape [48,49]. The curvature of the bending modes of a cantilever beam is largest near the clamped end and alternates along the beam, with the number of curvature maxima and nodes increasing

with the mode order. A defect located near a curvature maximum therefore produces a large frequency shift, whereas a defect located near a curvature node produces a very small one, even in a high-order mode. This explains why the most responsive mode changed with defect location and depth (Figure 3), and why modes such as f_5 showed large shifts at some locations and almost none at others, as at 100 and 250 mm (Table 1). The same mechanism is consistent with the consistency results. Where the curvature of a mode at the defect position is low, the frequency shifts are small and comparable to the measurement error, so their progression with defect depth cannot be resolved and the monotonic condition of Equation (6) may not be satisfied. This is the likely origin of the non-monotonic behavior of f_5 at 100 and 250 mm. In contrast, f_7 produced shifts of at least 100 Hz at 3 mm at all six locations, which is consistent with none of the examined locations being close to a curvature node of this mode and with its $C_7 = 1$. Similarly, the low response of f_8, with shifts not exceeding 44 Hz at 3 mm, is consistent with the examined locations lying in low-curvature regions of this mode. Since mode shapes were not measured in this study, these interpretations are consistent with the data but are not proven by them. They also indicate that the sensitivity and consistency rankings depend on the position of the defects relative to the curvature of each mode, and should not be extended to other defect locations without verification.

Overall, Figure 4 demonstrates that modal sensitivity and monotonic consistency are complementary selection criteria: their joint consideration identifies f_7 as the most balanced preliminary candidate, f_2 and f_4 as supporting modes, and f_8 as the least informative, suggesting that, subject to validation, future monitoring procedures for beam-like components might be simplified by prioritizing selected modes rather than treating all available modes equally. Practical implementation will also depend on sensor preparation and signal quality, since thermal annealing and Metglas material selection have been shown to influence the magnetic signal output of magnetoelastic ribbons [66–68]. The scope of these results is limited by the experimental conditions. The specimens were idealized aluminum cantilever beams with a single machined V-notch defect, one material, one geometry, and one clamping arrangement, and the measurements were performed in a laboratory setting. The results apply to defects located 50–300 mm from the clamped end, with depths of 1–3 mm (12–37% of the beam thickness). A machined notch also remains open during vibration, whereas a real fatigue crack may open and close, which can reduce its effect on the natural frequencies. Operational loads, temperature variations, changes in connection and boundary conditions, external vibration sources, multiple defects, and other environmental variables were not considered, and each of these can alter natural frequencies independently of damage. Neither measured mode shapes nor numerical simulations were available to verify the frequency-change mechanism directly, and the effect of mode selection on damage-identification performance was not evaluated, since selecting the modes and testing the identification on the same 18 single-specimen configurations would be circular.

The prioritization reported here is therefore a preliminary screening of the measured dataset. Its transfer to industrial components and practical monitoring requires validation on independent specimens, other geometries and boundary conditions, realistic damage, diagnostic thresholds, classification performance, and operating conditions [69].

The influence of environmental conditions on the magnetoelastic readout was not evaluated systematically in this study, but some considerations follow from the sensing material and from the experimental experience. The Metglas 2826MB3 ribbons have a Curie temperature of 353 C [41], which sets the upper limit for their magnetic response, so ambient temperature fluctuations, which are far below this value, are not expected to alter the behavior of the sensor significantly. Consistently, during the present experiments, which were performed under stable laboratory conditions, no fluctuations in the sensor readings

were observed when the temperature changed. The conditions that are more likely to affect the sensor are harsh ones, such as high humidity or marine environments, in which the corrosive action of salt water can degrade the ribbon itself, so that use in such environments would require protection of the sensor, which was not examined here. Temperature may still influence the natural frequencies of the beam through its elastic modulus, and mechanical noise from industrial machinery may add spectral components that overlap or mask the modal peaks. Neither effect was evaluated in this study, and both should be tested before the approach is applied outside the laboratory. Validation under realistic operational and environmental conditions requires a new experimental campaign, which is beyond the scope of this re-analysis of existing data. It is the primary objective of future work, together with re-clamping and independent specimens.

4. Conclusions

This study examined the individual response of the first eight bending modes of aluminum-alloy cantilever beams to a single crack-like defect at six locations and three depths. The frequency shifts generally increased with defect depth, but their magnitude depended strongly on the mode and on the defect location. Rather than demonstrating mode-dependent sensitivity, which is already well established, the study contributes a joint sensitivity-consistency screening of individual modes. This screening separated modes that were strongly responsive from those that also followed increasing damage severity reliably: f_7 combined the highest mean sensitivity, comparable to those of f_5 and f_6, with consistent behavior at all six locations, f_2 and f_4 were consistent but less sensitive, f_5 was sensitive but location dependent, and f_8 was the least informative at the examined locations.

These findings should be interpreted with several limitations in mind. First, the evidence comes from one specimen per configuration. The five repeated measurements quantify only the repeatability of the measurement (below 1 Hz), whereas variability due to re-clamping, sensor attachment, and differences between specimens was not quantified and may be larger. Second, the differences in mean sensitivity among f_5, f_6 and f_7 are small, and they depended on which defect locations were included, so the sensitivity alone does not establish the superiority of f_7; its preference rests on the combination with its consistency.

Third, the modal-curvature interpretation indicates that both the sensitivity and the consistency rankings are conditional on the position of the examined defects relative to the curvature of each mode. The prioritization of f_7 and the low priority of f_8 should therefore not be extended to other defect locations without checking the modal curvature at the expected positions, and since mode shapes were not measured, this interpretation is consistent with the data but not proven by them. Fourth, the consistency ratio is based on only six locations and three depths, and the analysis was descriptive, so no inferential statistics, diagnostic thresholds, or classification performance were established.

Finally, the specimens were idealized laboratory beams of a single material, geometry and clamping arrangement, each with a single machined defect, which differs from a real fatigue crack. Operational loads, temperature variations, changes in connection conditions, external vibration sources, and multiple defects were not considered, so the results should not be generalized to industrial components or practical monitoring. Future work should include measurements on independent specimens with paired pre-damage baselines and repeated clamping, other geometries and boundary conditions, a denser sampling of defect positions, realistic and multiple damage, measured mode shapes and numerical simulations, a quantitative comparison with other mode-selection approaches and of the damage-identification performance with and without mode selection on independent data, and operational and environmental variations, including corrosive conditions and mechanical noise, before the proposed mode-prioritization approach is considered for monitoring applications.

https://doi.org/10.3390/industries1020013

Funding: This research received no external funding.

Institutional Review Board Statement: Not applicable.

Informed Consent Statement: Not applicable.

Data Availability Statement: The mean modal frequencies analyzed in this study are provided in Table 1. Additional materials are available from the author on reasonable request.

Acknowledgments: The author thanks Dimitris Kouzoudis for helpful discussions concerning the original experimental dataset. During the preparation of this work, the author used AI tools, including GPT-5.3-mini model and Gemini 3, to improve the readability and quality of the language. After using these tools, the author thoroughly reviewed and revised the content as needed and accepts full responsibility for the final version of the publication.

Conflicts of Interest: The author declares no conflicts of interest.

References

1. Kralovec, C.; Schagerl, M. Review of structural health monitoring methods regarding a multi-sensor approach for damage assessment of metal and composite structures. *Sensors* **2020**, *20*, 826. [CrossRef] [PubMed]
2. Lei, Y.; Li, N.; Guo, L.; Li, N.; Yan, T.; Lin, J. Machinery health prognostics: A systematic review from data 407 acquisition to RUL prediction. *Mech. Syst. Signal Process.* **2018**, *104*, 799–834. [CrossRef]
3. Dadfarnia, M.; Sharp, M.E.; Herrmann, J.W. Comprehensive evaluations of condition monitoring-based technologies in industrial maintenance: A systematic review. *J. Manuf. Syst.* **2025**, *82*, 449–477. [CrossRef]
4. Farrar, C.R.; Worden, K. An introduction to structural health monitoring. *Philos. Trans. R. Soc. A Math. Phys. Eng. Sci.* **2007**, *365*, 303–315. [CrossRef] [PubMed]
5. Worden, K.; Farrar, C.R.; Manson, G.; Park, G. The fundamental axioms of structural health monitoring. *Proc. R. Soc. A Math. Phys. Eng. Sci.* **2007**, *463*, 1639–1664. [CrossRef]
6. Cawley, P. Structural health monitoring: Closing the gap between research and industrial deployment. *Struct. Health Monit.* **2018**, *17*, 1225–1244. [CrossRef]
7. Tibaduiza Burgos, D.A.; Gomez Vargas, R.C.; Pedraza, C.; Agis, D.; Pozo, F. Damage identification in structural health monitoring: A brief review from its implementation to the use of data-driven applications. *Sensors* **2020**, *20*, 733. [CrossRef] [PubMed]
8. Kot, P.; Muradov, M.; Gkantou, M.; Kamaris, G.S.; Hashim, K.; Yeboah, D. Recent advancements in non-destructive testing techniques for structural health monitoring. *Appl. Sci.* **2021**, *11*, 2750. [CrossRef]
9. Hannan, M.A.; Hassan, K.; Jern, K.P. A review on sensors and systems in structural health monitoring: Current 422 issues and challenges. *Smart Struct. Syst.* **2018**, *22*, 509–525.
10. Sony, S.; Laventure, S.; Sadhu, A. A literature review of next-generation smart sensing technology in structural health monitoring. *Struct. Control Health Monit.* **2019**, *26*, e2321. [CrossRef]
11. Abdulkarem, M.; Samsudin, K.; Rokhani, F.Z.; Rasid, M.F.A. Wireless sensor network for structural health monitoring: A contemporary review of technologies, challenges, and future direction. *Struct. Health Monit.* **2020**, *19*, 693–735. [CrossRef]
12. Sofi, A.; Regita, J.J.; Rane, B.; Lau, H.H. Structural health monitoring using wireless smart sensor network–An overview. *Mech. Syst. Signal Process.* **2022**, *163*, 108113. [CrossRef]
13. Lynch, J.P.; Loh, K.J. A summary review of wireless sensors and sensor networks for structural health monitoring. *Shock. Vib. Dig.* **2006**, *38*, 91–128. [CrossRef]
14. Mardanshahi, A.; Sreekumar, A.; Yang, X.; Barman, S.K.; Chronopoulos, D. Sensing techniques for structural health monitoring: A state-of-the-art review on performance criteria and new-generation technologies. *Sensors* **2025**, *25*, 1424. [CrossRef] [PubMed]
15. Alvandi, A.; Cremona, C. Assessment of vibration-based damage identification techniques. *J. Sound Vib.* **2006**, *292*, 179–202. [CrossRef]
16. Yan, Y.; Cheng, L.; Wu, Z.; Yam, L. Development in vibration-based structural damage detection technique. *Mech. Syst. Signal Process.* **2007**, *21*, 2198–2211. [CrossRef]
17. Avci, O.; Abdeljaber, O.; Kiranyaz, S.; Hussein, M.; Gabbouj, M.; Inman, D.J. A review of vibration-based damage detection in civil structures: From traditional methods to Machine Learning and Deep Learning applications. *Mech. Syst. Signal Process.* **2021**, *147*, 107077. [CrossRef]
18. Montalvão, D.; Maia, N.M.M.; Ribeiro, A.M.R. A review of vibration-based structural health monitoring with special emphasis on composite materials. *Shock. Vib. Dig.* **2006**, *38*, 295–324. [CrossRef]
19. Carden, E.P.; Fanning, P. Vibration based condition monitoring: A review. *Struct. Health Monit.* **2004**, *3*, 355–377. [CrossRef]

20. Doebling, S.W.; Farrar, C.R.; Prime, M.B. A summary review of vibration-based damage identification methods. *Shock. Vib. Dig.* **1998**, *30*, 91–105. [CrossRef]
21. Fan, W.; Qiao, P. Vibration-based damage identification methods: A review and comparative study. *Struct. Health Monit.* **2011**, *10*, 83–111. [CrossRef]
22. Curadelli, R.; Riera, J.; Ambrosini, D.; Amani, M. Damage detection by means of structural damping identification. *Eng. Struct.* **2008**, *30*, 3497–3504. [CrossRef]
23. Bandara, R.P.; Chan, T.H.; Thambiratnam, D.P. Structural damage detection method using frequency response functions. *Struct. Health Monit.* **2014**, *13*, 418–429. [CrossRef]
24. Deraemaeker, A.; Reynders, E.; De Roeck, G.; Kullaa, J. Vibration-based structural health monitoring using output-only measurements under changing environment. *Mech. Syst. Signal Process.* **2008**, *22*, 34–56. [CrossRef]
25. Elshafey, A.; Marzouk, H.; Gu, X.; Haddara, M.; Morsy, R. Use of fiber Bragg grating array and random decrement for damage detection in steel beam. *Eng. Struct.* **2016**, *106*, 348–354. [CrossRef]
26. Erazo, K.; Sen, D.; Nagarajaiah, S.; Sun, L. Vibration-based structural health monitoring under changing environmental conditions using Kalman filtering. *Mech. Syst. Signal Process.* **2019**, *117*, 1–15. [CrossRef]
27. Salawu, O.S. Detection of structural damage through changes in frequency: A review. *Eng. Struct.* **1997**, *19*, 718–723. [CrossRef]
28. Ostachowicz, W.M.; Krawczuk, M. Analysis of the effect of cracks on the natural frequencies of a cantilever beam. *J. Sound Vib.* **1991**, *150*, 191–201. [CrossRef]
29. Nandwana, B.P.; Maiti, S.K. Detection of the location and size of a crack in stepped cantilever beams based on measurements of natural frequencies. *J. Sound Vib.* **1997**, *203*, 435–446. [CrossRef]
30. Cawley, P.; Adams, R.D. The location of defects in structures from measurements of natural frequencies. *J. Strain Anal. Eng. Des.* **1979**, *14*, 49–57. [CrossRef]
31. Rizos, P.F.; Aspragathos, N.; Dimarogonas, A.D. Identification of crack location and magnitude in a cantilever beam from the vibration modes. *J. Sound Vib.* **1990**, *138*, 381–388. [CrossRef]
32. Patil, D.P.; Maiti, S.K. Detection of multiple cracks using frequency measurements. *Eng. Fract. Mech.* **2003**, *70*, 1553–1572. [CrossRef]
33. Vakil-Baghmisheh, M.T.; Peimani, M.; Sadeghi, M.H.; Ettefagh, M.M. Crack detection in beam-like structures using genetic algorithms. *Appl. Soft Comput.* **2008**, *8*, 1150–1160. [CrossRef]
34. Mazanoglu, K.; Sabuncu, M. A frequency based algorithm for identification of single and double cracked beams via a statistical approach used in experiment. *Mech. Syst. Signal Process.* **2012**, *30*, 168–185. [CrossRef]
35. Maghsoodi, A.; Ghadami, A.; Mirdamadi, H.R. Multiple-crack damage detection in multi-step beams by a novel local flexibility-based damage index. *J. Sound Vib.* **2013**, *332*, 294–305. [CrossRef]
36. Owolabi, G.M.; Swamidas, A.S.J.; Seshadri, R. Crack detection in beams using changes in frequencies and amplitudes of frequency response functions. *J. Sound Vib.* **2003**, *265*, 1–22. [CrossRef]
37. Hou, C.; Lu, Y. Experimental study of crack identification in thick beams with a cracked beam element model. *J. Eng. Mech.* **2017**, *143*, 04017020. [CrossRef]
38. Khatir, S.; Dekemele, K.; Loccufier, M.; Khatir, T.; Wahab, M.A. Crack identification method in beam-like structures using changes in experimentally measured frequencies and Particle Swarm Optimization. *Comptes Rendus Méc.* **2018**, *346*, 110–120. [CrossRef]
39. Grimes, C.A.; Roy, S.C.; Rani, S.; Cai, Q. Theory, instrumentation and applications of magnetoelastic resonance sensors: A review. *Sensors* **2011**, *11*, 2809–2844. [CrossRef] [PubMed]
40. Samourgkanidis, G.; Kouzoudis, D. Experimental detection by magnetoelastic sensors and computational analysis with finite elements, of the bending modes of a cantilever beam with minor damage. *Sens. Actuators A Phys.* **2018**, *276*, 155–164. [CrossRef]
41. Samourgkanidis, G.; Kouzoudis, D. A pattern matching identification method of cracks on cantilever beams through their bending modes measured by magnetoelastic sensors. *Theor. Appl. Fract. Mech.* **2019**, *103*, 102266. [CrossRef]
42. Samourgkanidis, G.; Kouzoudis, D. Characterization of magnetoelastic ribbons as vibration sensors based on the measured natural frequencies of a cantilever beam. *Sens. Actuators A Phys.* **2020**, *301*, 111711. [CrossRef]
43. Samourgkanidis, G.; Kouzoudis, D. Magnetoelastic ribbons as vibration sensors for real-time health monitoring of rotating metal beams. *Sensors* **2021**, *21*, 8122. [CrossRef] [PubMed]
44. Kouzoudis, D.; Samourgkanidis, G.; Tapeinos, C.I. Contactless Detection of Natural Bending Frequencies Using Embedded Metallic-Glass Ribbons inside Plastic Beams Made by 3-D Printing. *Recent Prog. Mater.* **2021**, *3*, 1–12. [CrossRef]
45. Tapeinos, C.I.; Kamitsou, M.D.; Dassios, K.G.; Kouzoudis, D.; Christogerou, A.; Samourgkanidis, G. Contactless and Vibration-Based Damage Detection in Rectangular Cement Beams Using Magnetoelastic Ribbon Sensors. *Sensors* **2023**, *23*, 5453. [CrossRef] [PubMed]
46. Tapeinos, C.I.; Kouzoudis, D.; Varvatsoulis, K.; Vázquez, M.; Samourgkanidis, G. Microwire vs. Micro-Ribbon Magnetoelastic Sensors for Vibration-Based Structural Health Monitoring of Rectangular Concrete Beams. *Sensors* **2025**, *25*, 3590. [CrossRef] [PubMed]

47. Samourgkanidis, G. Magnetoelastic Resonance Sensing for Structural Health Monitoring of Cementitious Materials. *Magnetism* **2026**, *6*, 21. [CrossRef]
48. Liu, Y.X.; Zhang, W.W.; Ma, H.W. Application of the higher modes to crack identification in a cantilever beam. *Key Eng. Mater.* **2007**, *347*, 595–600. [CrossRef]
49. Gillich, G.; Praisach, Z.; Abdel Wahab, M.; Vasile, O. Localization of transversal cracks in sandwich beams and evaluation of their severity. *Shock. Vib.* **2014**, *2014*, 607125. [CrossRef]
50. Soliman, E.S.M.M. Behavior of cracked Euler–Bernoulli beam and inverse problem for assessing crack severity. *Noise Vib. Worldw.* **2022**, *53*, 104–119. [CrossRef]
51. Sutar, M.K.; Pattnaik, S. Vibration characteristics of a cracked cantilever beam under free vibration. *Noise Vib. Worldw.* **2010**, *41*, 16–21. [CrossRef]
52. Sayyad, F.; Kumar, B. Theoretical and experimental study for identification of crack in cantilever beam by measurement of natural frequencies. *J. Vib. Control* **2011**, *17*, 1235–1240. [CrossRef]
53. Barad, K.H.; Sharma, D.; Vyas, V. Crack detection in cantilever beam by frequency based method. *Procedia Eng.* **2013**, *51*, 770–775. [CrossRef]
54. Mellel, N.; Ouali, M.; Dougdag, M.; Mohamedi, B. Experimental damage localization in beam by using natural frequency distribution and modal strain energy change ratio based methods. *J. Vibroeng.* **2015**, *17*, 1203–1217. [CrossRef]
55. Altunış¸ık, A.C.; Okur, F.Y.; Kahya, V. Modal parameter identification and vibration based damage detection of a multiple cracked cantilever beam. *Eng. Fail. Anal.* **2017**, *79*, 154–170. [CrossRef]
56. Chinka, S.S.B.; Putti, S.R.; Adavi, B.K. Modal testing and evaluation of cracks on cantilever beam using mode shape curvatures and natural frequencies. *Structures* **2021**, *32*, 1386–1397. [CrossRef]
57. Koh, B.; Dyke, S. Structural health monitoring for flexible bridge structures using correlation and sensitivity of modal data. *Comput. Struct.* **2007**, *85*, 117–130. [CrossRef]
58. Fan, W.; Qiao, P. A strain energy-based damage severity correction factor method for damage identification in plate-type structures. *Mech. Syst. Signal Process.* **2012**, *28*, 660–678. [CrossRef]
59. Mao, L.; Lu, Y. Selection of optimal artificial boundary condition (ABC) frequencies for structural damage identification. *J. Sound Vib.* **2016**, *374*, 245–259. [CrossRef]
60. Xu, M.; Wang, S.; Jiang, Y. Structural damage identification by a cross modal energy sensitivity based mode subset selection strategy. *Mar. Struct.* **2021**, *77*, 102968. [CrossRef]
61. Liu, Z.; Huang, J.; Wu, S.; Yu, S.; Dong, Z.; Guo, L. Damage identification methodology for composites via adaptive mode selection and unbiased weighted curvature. *Thin-Walled Struct.* **2026**, *226*, 114868. [CrossRef]
62. Wang, S. Damage detection in offshore platform structures from limited modal data. *Appl. Ocean. Res.* **2013**, *41*, 48–56. [CrossRef]
63. Chen, W.; Zhao, W.; Yang, H.; Chen, X. Damage detection based on optimized incomplete mode shape and frequency. *Acta Mech. Solida Sin.* **2015**, *28*, 74–82. [CrossRef]
64. Pérez, J.E.R.; Rodríguez, R.; Vázquez-Hernández, A.O. Damage detection in offshore jacket platforms with limited modal information using the damage submatrices method. *Mar. Struct.* **2017**, *55*, 78–103. [CrossRef]
65. Samourgkanidis, G. Reduced-Parameter Damage Detection in Cantilever Beams Using Magnetoelastically Measured Bending Frequencies. *Front. Built Environ.* **2026**, *12*, 1978290. [CrossRef]
66. Kouzoudis, D.; Baimpos, T.; Samourgkanidis, G. A new method for the measurement of the diffusion coefficient of adsorbed vapors in thin zeolite films, based on magnetoelastic sensors. *Sensors* **2020**, *20*, 3251. [CrossRef] [PubMed]
67. Samourgkanidis, G.; Varvatsoulis, K.; Kouzoudis, D. The Effect of the Thermal Annealing Process to the Sensing Performance of Magnetoelastic Ribbon Materials. *Sustainability* **2021**, *13*, 13947. [CrossRef]
68. Samourgkanidis, G.; Kouzoudis, D.; Charalampous, P.; Adnan, E. Signal Enhancement in Magnetoelastic Ribbons Through Thermal Annealing: Evaluation of Magnetic Signal Output in Different Metglas Materials. *Sensors* **2025**, *25*, 3722. [CrossRef] [PubMed]
69. Sohn, H. Effects of environmental and operational variability on structural health monitoring. *Philos. Trans. R. Soc. A Math. Phys. Eng. Sci.* **2007**, *365*, 539–560. [CrossRef] [PubMed]

Disclaimer/Publisher's Note: The statements, opinions and data contained in all publications are solely those of the individual author(s) and contributor(s) and not of MDPI and/or the editor(s). MDPI and/or the editor(s) disclaim responsibility for any injury to people or property resulting from any ideas, methods, instructions or products referred to in the content.